Journal of Trace Elements in Medicine and Biology 24 (2010) 58–66

Contents lists available at ScienceDirect

Journal of Trace Elements in Medicine and Biology

journal homepage: www.elsevier.de/jtemb

Pathobiochemistry

Iron absorption and distribution in TNF$^{\Delta ARE/+}$ mice, a model of chronic inflammation

Klaus Schümann [a,*], Nadia Herbach [b], Christina Kerling [a], Markus Seifert [c], Carine Fillebeen [d], Isabella Prysch [a], Jens Reich [e], Günter Weiss [c], Kostas Pantopoulos [d]

[a] Science Centre Weihenstephan, Technical University Munich, Gregor Mendelstr. 2; 85350 Freising, Germany
[b] Animal Pathology, Ludwig-Maximilians-University, Veterinär Str. 13, 80539 München, Germany
[c] Department of Internal Medicine I, Clinical Immunology and Infectious Diseases, Medical University of Innsbruck, Anichstr. 35, 6020 Innsbruck, Austria
[d] Lady Davis Institute for Medical Research and Department of Medicine, McGill University, 3755 Cote St. Catherine Road, Montreal, Quebec, Canada H3T 1E2
[e] Max-Delbrueck-Centre of Molecular Medicine, Robert-Rössle-Straße 10, 13125 Berlin-Buch, Germany

ARTICLE INFO

Article history:
Received 27 April 2009
Accepted 13 October 2009

Keywords:
Inflammation
TNF$^{\Delta ARE/+}$ mice
Iron-absorption
Iron-distribution
Proteins of iron homoeostasis

ABSTRACT

Hemizygous TNF$^{\Delta ARE/+}$ mice are a murine model for chronic inflammation. We utilized these animals to study iron-kinetics and corresponding protein expression in an iron-deficient and iron-adequate setting. ^{59}Fe-absorption was determined in ligated duodenal loops *in vivo*. Whole body distribution of i.v. injected ^{59}Fe was analysed, and the organ specific expression of ferroportin, transferrin receptor-1, hepcidin and duodenal DMT-1 was quantified by real-time PCR and Western blotting.

Duodenal ^{59}Fe-lumen-to-body transport was not affected by the genotype. Duodenal ^{59}Fe-retention was increased in TNF$^{\Delta ARE/+}$ mice, suggesting higher ^{59}Fe-losses with defoliated enterocytes. Iron-deficiency increased duodenal ^{59}Fe-lumen-to-body transport, and higher duodenal ^{59}Fe-tissue retention went along with higher duodenal DMT-1, ferroportin, and liver hepcidin expression. TNF$^{\Delta ARE/+}$ mice significantly increase their ^{59}Fe-content in inflamed joints and ilea, and correspondingly reduce splenic ^{59}Fe-content. Leukocyte infiltrations in the joints suggest a substantial shift of iron-loaded RES cells to inflamed tissues as the underlying mechanism. This finding was paralleled by increased non-haem iron content in joints and reduced haemoglobin and haematocrit concentrations in TNF$^{\Delta ARE/+}$ mice.

In conclusion, erythropoiesis in inflamed TNF$^{\Delta ARE/+}$ mice could be iron-limited due to losses with exfoliated iron-loaded enterocytes and/or to increased iron-retention in RES cells that shift from the spleen to inflamed tissues.

Introduction

Chronic inflammation is frequently associated with hypoferremia due to iron retention within the reticuloendothelial system and decreased intestinal iron absorption [1]. This is achieved by the effects of cytokines and acute phase proteins on cellular iron transport pathways. The master regulator of iron homoeostasis, hepcidin, is an acute phase peptide induced by inflammation [2]. Hepcidin binds to the only known iron exporter, ferroportin, thereby causing its internalisation and degradation which results in cellular iron retention [3]. In addition, cytokines enhance the uptake of transferrin and non-transferrin bound iron into macrophages [4,5], stimulate iron storage within these cells by inducing the expression of the iron storage protein ferritin [6,7], and inhibit iron export by inhibition of ferroportin mRNA expression [4,8]. Moreover, macrophages can produce hepcidin which then targets ferroportin in an autocrine fashion [9]. The binding of hepcidin to ferroportin reduces duodenal iron absorption [10], while tumour necrosis factor-alpha (TNF-α) inhibits duodenal iron absorption by a hepcidin-independent mechanism [11]. These events are thought to further contribute to circulatory hypoferremia and iron-limited erythropoiesis. In conjunction with inflammation-mediated inhibition of erythropoiesis and an impaired biological activity of erythropoietin, these events are assumed to promote anaemia of chronic disease (ACD) [1,12]. In inflammatory bowel diseases (IBD), chronic intestinal blood loss from the affected segments may further aggravate anaemia, leading to a combination of ACD with true iron deficiency [13,14].

TNF$^{\Delta ARE}$ mice, developed by Kollias and coworkers, constitute a genetic model of IBD and chronic arthritis [15]. The phenotype of

Abbreviations: ACD, anaemia of chronic disease; ECL, enhanced chemiluminescence; IBD, inflammatory bowel diseases; IRP2, iron regulatory protein 2; PBS, phosphate buffered saline; PBST, phosphate buffered saline Tween; RES, reticuloendothelial system; TfR1, transferrin receptor 1; TNF-α, tumour necrosis factor-alpha

* Corresponding author at: Zentralinstitut für Ernährung und Lebensmittelforschung, Sekretariat Prof. Daniel, Am Forum 5, 85350 Freising-Weihenstephan, Germany.
E-mail address: kschuemann@schuemann-muc.de (K. Schümann).

0946-672X/$ - see front matter © 2009 Elsevier GmbH. All rights reserved.
doi:10.1016/j.jtemb.2009.10.002

hemizygous $TNF^{\Delta ARE/+}$ mice is milder and allows to investigate the impact of inflammation on intestinal iron absorption *in vivo*, without using proinflammatory chemicals (e.g. dextrane sulphate sodium; [16]) that may cause confounding pleiotropic effects. By employing this model, we investigated the effects of chronic inflammation and iron-deficiency on functional variables (duodenal ^{59}Fe-absorption, haemoglobin concentration, hepatic and splenic non-haem iron content, ^{59}Fe-whole body distribution) and on the expression of duodenal, splenic, and hepatic proteins of iron homoeostasis [duodenal DMT-1, hepcidin, ferroportin, ferritin, and transferrin receptor-1 (TfR1)] on the mRNA and/or protein level. These variables were compared between iron-deficient and iron-adequate $TNF^{\Delta ARE/+}$ mice and their wild-type litter mates.

Materials and methods

Animals

The experiments were performed according to the rules of animal care (Approval: Regierung von Oberbayern: AZ 209.1/211-2531-109/03 and AZ 55.2-1-54-2531-74-06). Hemizygous $TNF^{\Delta ARE/+}$ mice and wild type littermates were housed in macrolone cages (5–8 animals/cage, 12:12 h light–dark cycle: 0600–1800 h; 22 ± 1 °C, 60 ± 5% humidity). They entered the experiments at an age of 12–14 weeks. Mice utilized for photometrical analysis of non-haem iron were 18 weeks old. Iron deficiency was induced by intake of an iron-deficient diet (C1038, Altrumin, Lage, Germany, total Fe-content: 6 mg Fe/kg) and distilled water *ad libitum* for 5 weeks during rapid growth [17]. Iron-adequate animals received a corresponding iron-adequate diet (C1000, Altrumin, total Fe-content: 180 mg Fe/kg).

Analysis of body iron status

Haematocrit and haemoglobin concentrations were measured by the microhaematocrit method (no. 749311, Brand, Wertheim, Germany; Haematocrit-centrifuge 2104, Hettlich, Tuttlingen, Germany) and the cyanmethaemoglobin method (reagent: Bioanalytic 4001, Umrich, Freiburg, Germany; photometer: UV-DK-20, Beckmann, München, Germany), respectively. To determine hepatic and splenic non-haem iron content, tissue samples (approx. 300–400 mg) were cut into pieces (approx. 1 mm^3) and agitated in acid-mix (6 mol/L HCl, 20% TCA; v/v) to extract non-haem iron [18]. After incubation (65 °C, 20 h) non-haem iron was determined photometrically in diluted acid-mix by the use of a commercial test-kit (Feren-B, Bioanalytic, Umrich/Freiburg, Germany).

Histology

Animals were fixed by immersion in 4% buffered formalin for 24 h. The phalanges one and two of the right hind leg were removed in the proximal tarsal joint, processed in a Citadel 1000 (Shandon, Germany), and subsequently embedded in plastic, containing hydroxymethylmethacrylate (Fluka Chemie, Germany) and methylmethacrylate (Riedel de Haën, Germany) as described elsewhere in detail [19]. Approximately 1.5 μm thick plastic sections were cut on a Reichert-Jung 2050 rotary microtome (Cambridge Instruments, Germany) and stained with hematoxylin and eosin.

Determination of duodenal iron transport

Duodenal iron absorption was determined as described previously [20]. In short, mice were fasted overnight. A tied-off duodenal segment (~2 cm) was flushed with saline, filled *in situ* with 50–100 μL of perfusion medium (125 mmol/L NaCl, 3.5 mmol/L KCl, 10 mmol/L D-Glucose, 16 mmol/L Na-HEPES (N-2-hydroxyethylpiperazine-N′-2-ethylenesulfonic acid, pH 7.4), containing 100 μmol/L $^{59}Fe^{3+}$-nitrilotriacetate 1:2. (NEZ 37, Amersham, Germany; anaesthesia: Metedomidinhydrochloride/Ketaminhydrochlorid, both Pharmacia GmbH, Karlsruhe, Germany; s.c. 0.33 mg/66 mg/kg). The ligated duodenal segment was removed after 10 min of incubation, and after ligation of mesenteric blood supply. The segments' lumen was extensively flushed with stop-medium, opened, blotted, and counted in a well-type gamma-counter (1282 Compugamma CS, LKB, Wallac, Finland) after determining its length and dry weight. The radioactivity transferred to the body was measured in a whole body counter for small animals (Type AW3, Münchener Apparatebau, Unterföhring, Germany), and ^{59}Fe transport was expressed as pmol ^{59}Fe/cm/min.

Proteins of iron homoeostasis

Duodenal DMT-1, hepcidin, ferroportin, transferrin receptor-1 (TfR1), iron regulatory protein-2 (IRP2), and ferritin, were determined on the mRNA and/or protein levels in duodena, liver, and spleen. For the Western blots the duodenum was flushed and rinsed with isotonic saline *in situ* and snap frozen in liquid nitrogen after removal from the living mice within 4 s. Liver and spleen were removed after death and frozen immediately. Materials for real-time PCR were separated from the same organs and stored in RNA-later® (No AM 7020 Ambion Applied Biosystems, TX, USA).

Description of real time PCR

Preparation of total RNA and quantification of mRNA expression by Taq-Man real time RT-PCR following reverse transcription was performed as described earlier [21]. The following primers of Taq-Man probes were used: TfR: 5′-CGCTTTGGGTGCTGGTG-3′, 5′-GGGCAAGTTTCAACAGAAGACC-3′, 5′-CCCACACTGGACTTCGCCG-CA-3′; DMT-1: 5′-CCAGCCAGTAAGTTCAAGGATCC-3′, 5′-GCGTAG-CAGCTGATCTGGG-3′, 5′-TGGCCTCGCGCCCCAACA-3′, ferroportin: 5′-CTACCATTAGAAGGATTGAC CAGCT-3′, 5′-CAAATGTCATAATCT-GGCCGA-3′, 5′-CAACATCCTGGCCCCCA-TGGC-3′; hepcidin-1: 5′-TGTCTCCTGCTTCTCCTCCTTG-3′, 5′-AGCTCTGTAGT;CTGTCTCATCTGTT-GA-3′, 5′-CAGCCTGAGCAGCACCACCTATCTCC-3′. Murine primers and probes were purchased from Microsynth, the latter carrying 5′-FAM and 3′-BHQ1 labels. A standard curve with material from earlier experiments showing high expression levels for the mRNA under consideration was run along with every experiment. Values in Table 6 are given in percent of those determined in corresponding iron-adequate wild-type mice in each set of determinations.

Description of Western blot analysis

Total lysates were prepared by homogenization of nitrogen frozen tissues in RIPA buffer (150 mmol/L NaCl, 1% NP-40, 0.5% deoxycholic acid, 0.1% SDS, 50 mmol/L Tris pH 8.0) containing a cocktail of protease inhibitors (Sigma #P8340). For preparation of a membrane-enriched fraction, tissues were lysed using polytron in HEM buffer (20 mmol/L Hepes, pH 7.4, 1 mmol/L EDTA, 300 mmol/L mannitol containing protease inhibitors) and insoluble debris was discarded by low speed centrifugation. The membrane fraction was pelleted by centrifugation at 100,000*g* for 30 min and membranes were resuspended in HEM buffer. After determination of protein concentration with Bradford reagent (Biorad), 50 μg of lysates or 10 μg of membrane proteins were resolved by SDS-PAGE on 15% or 8% gels and transferred onto nitrocellulose filters. For ferroportin detection, samples were free of beta-mercaptoethanol and non-boiled before loading for PAGE.

The blots were saturated with 10% non-fat milk in PBS and probed with antibodies against IRP2 (a kind gift of B. Galy and M.W. Hentze; dilution 1:500), TfR1 (Zymed; dilution 1:1000), ferritin (Novus; dilution 1:1000), ferroportin (a kind gift of M. Knutson; dilution 1:250), DMT-1 (dilution: 1:500) or β-actin (Sigma; dilution 1:1000) [22,23]. For generation of a DMT-1 antibody, a rabbit was immunized with a recombinant polypeptide consisting of 8 repeats of amino acids 4-54 of DMT-1. Dilutions were in PBS containing 0.5% Tween 20 (PBST). Following wash with PBST, the blots with monoclonal TfR1 antibody were incubated with peroxidase-coupled rabbit anti-mouse IgG (1:5000 dilution), and the blots with polyclonal antibodies were incubated with peroxidase-coupled goat anti-rabbit IgG (1:10,000 dilution). Peroxidase-coupled antibodies were detected with the enhanced chemiluminescence (ECL) method, according to the manufacturer's instructions (Amersham).

Determination of ^{59}Fe-distribution and residual tissue blood content

The animals were intravenously injected with Fe-NTA(1:2) complex, solved in isotonic HEPES-buffered saline (pH 7.0), 0.2 μmol Fe/kg body weight, and labelled with ~2 μCi ^{59}Fe/animal (~10 μCi ^{59}Fe/animal for donors of ^{59}Fe-labelled erythrocytes) (NEZ 037, NEN Dreieich, Germany). Residual blood content in all organs and tissues including inflamed paws and tail samples was determined in TNF$^{\Delta ARE/+}$ and corresponding wild-type-mice after injection of ^{59}Fe-labelled whole blood as described earlier [24]. Iron-adequate TNF$^{\Delta ARE/+}$ mice and their wild-type litter mates were dissected 1 d or 14 d after intravenous ^{59}Fe-injection, the second representing steady-state conditions of ^{59}Fe-distribution. Before sacrifice, ^{59}Fe whole-body activity was determined along with the ^{59}Fe-activity in 25 μL of the injection solution in a whole body counter. Approx. 200 μL of blood was sampled from the abdominal vena cava, and the animals were euthanized and dissected. Representative samples of all organs and tissues were separated and sample weight determined (scales: PI-403, Denver Instruments Pinnacle, precision: 1 mg). ^{59}Fe-activity was measured in a well-type γ-counter (1282 Compugamma CS, LKB, Wallac, Finland).

Residual tissue blood content was assessed by injecting ^{59}Fe-labelled blood via the vena cava, determination of the erythrocyte-bound ^{59}Fe-activity in all organs and tissues, and relating its activity to that in μL of blood from the same mouse after a distribution period of 15 min as described earlier [24].

Subtraction method

The total ^{59}Fe in the organs and tissues was corrected for ^{59}Fe related to the estimated residual tissue blood content as described earlier [24]. This method relates the individually determined ^{59}Fe-concentration in 1 μL blood to the residual blood content in 1 g of tissue. The ^{59}Fe-fraction related to the residual blood thus determined was subtracted from total ^{59}Fe activity in all tissues.

Separation method

Tissue samples were minced with scissors and scalpel, homogenised in digitonine solution (130 mg digitonine/L, no. 4946.1, Roth, Karlsruhe, Germany; 20% weight/weight, 2 min, 20,000 rpm) and ultrasonicated for 10 min as described earlier [25]. ^{59}Fe radioactivity was determined in 313 μL of tissue homogenates and subsequently incubated with an equal volume of H_3PO_4 (85%, 9 mol/L, 37 °C, 20 min; Sigma, No. 466123) plus 125 μL of a saturated KH_2PO_4 (Sigma, no. 0662). After addition of 750 μL cyclohexanone (Sigma, no. 398241) the solution was intensely agitated for 5 min (Vortex, IKA Labortechnik VF, Staufen, Germany). After centrifugation (14,000 rpm, 15 min, Centrifuge Sigma 1–15 K, Steinheim, Germany), the mixture separated into a lower, inorganic phase containing ^{59}Fe-labelled non-haem iron, and an upper, organic phase containing haem-bound ^{59}Fe. ^{59}Fe was determined in both phases and added up to approx. 90% of ^{59}Fe determined in the homogenate before processing [25].

All chemicals were purchased from Sigma, and Merck, Darmstadt.

Statistics

Values of the different groups are presented as means ± standard deviation. Corresponding iron-deficient vs. iron-adequate or wild-type vs. TNF$^{\Delta ARE/+}$ mice were compared by unpaired Student *t*-test (WinSTAT®, Microsoft, USA). Homogeneity of variance was tested by the Bartlett-test. The level of significance for all comparisons was $p < 0.05$.

Results

Parameters of iron status (Table 1)

In mice used for investigating duodenal ^{59}Fe-absorption, hepatic and splenic non-haem iron content was significantly decreased in iron-deficiency. The liver showed no differences between corresponding wild-type and TNF$^{\Delta ARE/+}$ mice, while splenic non-haem iron content was significantly lower in TNF$^{\Delta ARE/+}$ mice of both iron statuses (Table 1a). Haemoglobin concentrations and haematocrit values were significantly lower in iron-deficient as compared to iron-adequate TNF$^{\Delta ARE/+}$ mice, and wild-type littermates. Haemoglobin concentrations were lower in TNF$^{\Delta ARE/+}$ mice, though differences did not reach significance in this small group. Haematocrit values, however, were significantly lower in TNF$^{\Delta ARE/+}$ mice irrespective of iron status (Table 1a). In a larger set of 25 iron-adequate mice, haemoglobin concentrations and

Table 1a
Parameters of iron status in mice from the absorption study.

	Hepatic non-haem iron (μg/g wet weight)	Spleenic non-haem iron (μg/g wet weight)	Haemoglobin (g/L)	Haematokrit (%)
TNF$^{\Delta ARE/+}$				
Iron-adequate	84.1 ± 30.6 (*n*=9)*	256.0 ± 69.8 (*n*=10)*	130 ± 18 (*n*=11)*	41 ± 5 (*n*=11)*
Iron-deficient	42.1 ± 11.7 (*n*=5)	59.2 ± 27.5 (*n*=10)	97 ± 36 (*n*=5)	32 ± 10 (*n*=5)
Wild-type				
Iron-adequate	99.0 ± 30.3 (*n*=7)*	526.7 ± 141.5 (*n*=19)*+	140 ± 16 (*n*=8)	46 ± 4 (*n*=8)+
Iron-deficient	35.4 ± 9.8 (*n*=5)	131.9 ± 35.4 (*n*=10) +	123 ± 15 (*n*=8)	45 ± 3 (*n*=7)+

* Significant differences between iron-adequate and iron-deficient mice.
\+ Significant differences between TNF$^{\Delta ARE/+}$ and wild-type-mice of corresponding iron status.

Table 1b
Parameters of iron status in iron-adequate $TNF^{\Delta ARE/+}$ and wild-type-mice (M ± SD, n=25).

	Hepatic non-haem iron (μg/g wet weight)	Haemoglobin (g/L)	Haematokrit (%)
$TNF^{\Delta ARE/+}$	94 ± 31	126 ± 19	40 ± 6
Wild-type	87 ± 22	138 ± 17^{+}	43 ± 4^{+}

Comparison between two corresponding groups of mice (unpaired Student t-test, $p < 0.05$).

$^{+}$ Significant differences between $TNF^{\Delta ARE}$- and wild-type-mice of corresponding iron status.

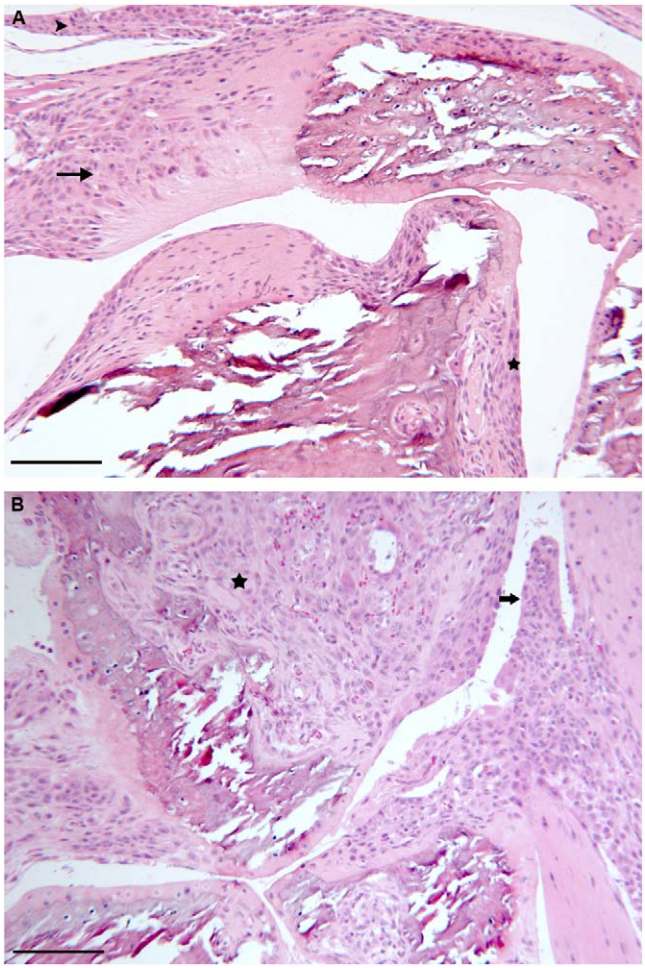

Fig. 1. . Tarso-metatarsal joint of a 25-week-old $TNF^{\Delta ARE/+}$ mouse: (A) Pannus covering the cartilage (asterisk) as well as mononuclear infiltration of the tendon (arrow) and tendon sheath (arrow head); (B) subchondral pannus formation (asterisk) is seen along with massive invasion of the synovium (arrow) with macrophages, lymphocytes, and neutrophilic granulocytes. Plastic embedded tissue, H&E stain, bar represents 100 μm.

haematocrit values were significantly lower in $TNF^{\Delta ARE/+}$ mice than in wild-type-mice, while hepatic non-haem iron, again, showed no significant differences (Table 1b).

Histology

$TNF^{\Delta ARE/+}$ mice (Fig. 1) exhibited severe joint alterations of the phalanges, including extensive diffuse invasion of the synovium with macrophages, lymphocytes, and few neutrophils. There was multifocal pannus formation, covering the cartilage, as well as subchondral pannus formation with bone destruction. Extensive fibrovascular proliferation around small islets of destructed bone, and invasion by numerous macrophages, multinucleated giant cells and some neutrophils were frequently evident. In addition, there were signs of severe tendinitis and tendosynovitis, characterized by infiltration of the tendon and tendon sheath with inflammatory cells.

Table 2
Duodenal ^{59}Fe-transport data.

	^{59}Fe-transport (lumen-to-body) (pmol/cm/min)	duodenal ^{59}Fe tissue retention (nmol ^{59}Fe/cm)
$TNF^{\Delta ARE/+}$		
Iron-adequate	4.4 ± 3.0 (n=8)*	0.61 ± 0.27 (n=8)*
Iron-deficient	37.3 ± 10.5 (n=5)	2.41 ± 0.56 (n=5)$^{+}$
Wild-type		
Iron-adequate	3.0 ± 1.7 (n=7)*	0.44 ± 0.13 (n=7)*
Iron-deficient	42.8 ± 3.0 (n=5)	1.52 ± 0.46 (n=5)

Comparison between 2 corresponding groups of mice (unpaired Student t-test, $p < 0.05$).

* Significant differences between iron-adequate and iron-deficient mice.

$^{+}$ Significant differences between $TNF^{\Delta ARE/+}$ and wild-type-mice of corresponding iron status.

Duodenal ^{59}Fe-transport in ligated loops in vivo (Table 2)

Duodenal lumen-to-body ^{59}Fe-transport was significantly increased in iron-deficiency, while no significant differences were observed between genotypes. Duodenal ^{59}Fe-tissue retention was significantly increased in iron-deficiency. It was also higher in $TNF^{\Delta ARE/+}$ mice as compared to wild-type litter mates, the difference reaching significance in iron-deficiency (Table 2).

Residual tissue blood content

The content of previously injected ^{59}Fe-labelled blood was higher in the inflamed hind-paws of $TNF^{\Delta ARE/+}$ mice (wild-type: 8.9 ± 0.7 μL blood/g w wt; $TNF^{\Delta ARE/+}$: 13.0 ± 3.7 μL blood/g w wt, p=0.13, n=3) and tail-tissue (wild-type: 10.1 ± 2.2 μL blood/g w wt; $TNF^{\Delta ARE/+}$: 17.6 ± 3.3 μL blood/g w wt, $p < 0.05$, n=3), though significance was only reached in tail tissue. Residual blood content in the other tissues (data not shown) exhibited no significant differences between wild-type- and $TNF^{\Delta ARE/+}$ -mice and was in the same order of magnitude as determined earlier for wild-type-C57BL6-mice [24]. These values for residual tissue blood content entered the calculation of ^{59}Fe-distribution (see Mat. & Meth., "subtraction method").

^{59}Fe distribution in adult $TNF^{\Delta ARE/+}$ and wild-type-mice (Table 3)

As early as 24 h after ^{59}Fe-injection, specific ^{59}Fe tissue contents determined by the "subtraction method" were significantly higher in fore- and hind-paws and, unexpectedly, also in the brain of $TNF^{\Delta ARE/+}$ mice. Fourteen days after injection, ^{59}Fe-tissue content was still significantly higher in paws and brain, but also in the ileum and in the duodenum of $TNF^{\Delta ARE/+}$ mice as compared to wild-types. Moreover, ^{59}Fe tissue content decreased significantly in duodenum, ileum, spleen, fur and bone within 14 days after injection (Table 3).

Significantly higher ^{59}Fe-retention in inflamed paws from $TNF^{\Delta ARE/+}$ mice than from controls was found by the "subtraction method" and by the "separation method". The "subtraction

Table 3
Specific ^{59}Fe-load in adult wild-type and TNF$^{\Delta ARE/+}$-mice, "subtraction method". M ± SD, [nmol ^{59}Fe/g wwt].

	Distribution interval: 1 day		Distribution interval: 14 days	
	Wild-type (n=7)	TNF$^{\Delta ARE/+}$ (n=7)	Wild-type (n=6)	TNF$^{\Delta ARE/+}$ (n=8)
Duodenum	0.226 ± 0.087	0.251 ± 0.097	0.016 ± 0.024^{+}	0.062 ± 0.032^{*+}
Ileum	0.298 ± 0.167	0.205 ± 0.098	0.023 ± 0.021^{+}	0.068 ± 0.035^{*+}
Heart	0.224 ± 0.155	0.185 ± 0.032	0.131 ± 0.083	0.178 ± 0.098
Liver	0.403 ± 0.145	0.345 ± 0.085	0.239 ± 0.122	0.288 ± 0.084
Spleen	0.899 ± 0.266	1.076 ± 0.313	0.235 ± 0.075^{+}	0.173 ± 0.051 $^{+}$
Kidney	0.209 ± 0.112	0.246 ± 0.111	0.169 ± 0.061	0.186 ± 0.064
Fur	0.084 ± 0.067	0.122 ± 0.077	0.008 ± 0.070	0.047 ± 0.033 $^{+}$
Fat	0.091 ± 0.090	0.077 ± 0.072	0.017 ± 0.032	0.067 ± 0.075
Brain	0.011 ± 0.005	0.019 ± 0.008*	0.010 ± 0.008	0.024 ± 0.009^{+}
Bone	0.635 ± 0.209	0.495 ± 0.139	0.101 ± 0.058^{+}	0.088 ± 0.046 $^{+}$
Muscle	0.022 ± 0.009	0.030 ± 0.017	0.020 ± 0.009	0.031 ± 0.029
Stomach	0.106 ± 0.076	0.100 ± 0.030	0.044 ± 0.035	0.062 ± 0.051
Fore-paws	0.051 ± 0.024	0.089 ± 0.026*	0.034 ± 0.023	0.082 ± 0.029*
Hind-paws	0.040 ± 0.013	0.068 ± 0.026*	0.034 ± 0.007	0.067 ± 0.016*
Tail	0.019 ± 0.007	0.019 ± 0.014	0.021 ± 0.007	0.015 ± 0.006

* Significant differences between corresponding wild-type- and TNF$^{\Delta ARE/+}$-mice.
$^{+}$ Significant differences between corresponding 1 day and 14 day distribution; unpaired Student t-test, $p \leq 0.05$.

Table 4
Comparison of ^{59}Fe-load in the inflamed tissues from iron-adequate, adult wild-type and TNF$^{\Delta ARE/+}$-mice, as determined by the "subtraction method" and "separation method"; distribution period: 14 days (nmol ^{59}Fe/g w wt), M ± SD, n=7, (unpaired Student t-test, $p < 0.05$).

	"Subtraction"		"Separation"	
	Wild-type" (n=5)	TNF$^{\Delta ARE/+}$ (n=7)	Wild-type (n=5)	TNF$^{\Delta ARE/+}$ (n=7)
Fore-paws	0.027 ± 0.017	0.089 ± 0.021*	0.020 ± 0.011	0.054 ± 0.021^{*+}
Hind-paws	0.031 ± 0.003	0.069 ± 0.015*	0.015 ± 0.004^{+}	0.073 ± 0.028*
Tail	0.019 ± 0.006	0.016 ± 0.006	0.013 ± 0.005	0.022 ± 0.007*

* Significant differences between corresponding wild-type- and TNF$^{\Delta ARE/+}$-mice.
$^{+}$ Significant differences between corresponding data from "subtraction method" vs. "separation method".

method" yielded higher results for non-haem-related ^{59}Fe tissue content in the fore-paws of TNF$^{\Delta ARE/+}$ mice and in the hind-paws of wild-types (Table 4).

Determination of tissue non-haem iron content

Photometric assessment of tissue non-haem iron content after acidic extraction of endogenous iron from the tissues in iron-adequate, adult wild-type- and TNF$^{\Delta ARE/+}$ mice agreed with the ^{59}Fe-distribution data. Photometric values were significantly higher in the tail-tissue (wild-type-mice: 13.8 ± 4.8 μg/g w wt, n=10; TNF$^{\Delta ARE/+}$ mice: 19.5 ± 5.2 μg/g w wt, n=14) and hind-paws (wild-type-mice: 23.2 ± 9.2 μg/g w wt, n=10; TNF$^{\Delta ARE/+}$ mice: 37.5 ± 6.9 μg/g w wt, n=14) from TNF$^{\Delta ARE/+}$ mice.

Expression of iron homoeostasis genes in different organs

Hepatic hepcidin-1 mRNA expression was significantly higher in iron-adequate than in iron-deficient mice in both, TNF$^{\Delta ARE/+}$ and wild-type mice (Table 5). Absolute values for hepcidin-1 expression in the spleen were 5 orders of magnitude lower than in the liver. Ferroportin mRNA levels were in the same order of magnitude in all three organs. Duodenal ferroportin mRNA levels were significantly increased in iron-deficiency, but showed no increments in TNF$^{\Delta ARE/+}$ as compared to wild-type-mice. While DMT-1 mRNA expression had a tendency to up-regulation in iron-deficient wild-type animals, no such effect was observed in TNF$^{\Delta ARE/+}$ mice. Hepatic ferroportin mRNA, in contrast, was significantly decreased in iron-deficient TNF$^{\Delta ARE/+}$ as compared to corresponding wild-type-mice and showed no significant differences between iron-adequate wild-type- and TNF$^{\Delta ARE/+}$ mice. No significant differences were seen in splenic ferroportin mRNA levels in response to differences in genotype or iron status. Duodenal transferrin-receptor (TfR1) mRNA was significantly increased in iron-deficient as compared to iron-adequate wild-type-mice. TfR1 mRNA was significantly increased in iron-deficient liver samples. Hepatic TfR1 was higher in iron-adequate and lower in iron-deficient TNF$^{\Delta ARE/+}$ as compared to wild-type-mice. TfR1 mRNA values in the spleen showed no differences in response to iron status or genotype (Table 5).

Densitometric quantification of Western blots (Table 6) revealed significantly increased ferroportin protein expression in iron-deficient duodena of both TNF$^{\Delta ARE/+}$ and wild-type-mice alike. Interestingly, iron-deficient duodena of TNF$^{\Delta ARE/+}$ mice expressed about 50% lower ferroportin levels as compared to wild-type littermates; nevertheless, this difference failed to reach statistical significance (p=0.16). Duodenal DMT-1 protein levels were significantly higher in iron-deficiency but showed no differences between genotypes. Hepatic ferroportin protein levels were significantly higher in iron-deficient than in iron-adequate wild-type mice. Iron-adequate TNF$^{\Delta ARE/+}$ mice showed significantly higher hepatic ferroportin values than the corresponding wild-type animals. Splenic ferroportin values were increased with iron-deficiency, reaching significance in wild-type-mice. Moreover, splenic ferroportin content in TNF$^{\Delta ARE/+}$ mice was higher than in wild-types, reaching significance in iron-deficiency. TfR1 protein levels were generally higher in iron-deficiency (Table 6) though,

Table 5
mRNA expression of proteins of iron metabolism in duodenum, spleen, and liver from $TNF^{\Delta ARE/+}$ mice (n=5) and wild-type-mice (n=5) (M ± SD).

Duodenum	**ferroportin**	**TfR1**	**DMT-1**
$TNF^{\Delta ARE/+}$			
Iron-adequate	54.3 ± 34.8*	103.6 ± 40.7	101.7 ± 25.0
Iron-deficient	380.1 ± 237.3	113.0 ± 49.3	102.0 ± 20.8
Wild-type			
Iron-adequate	100.0 ± 78.6*	100.0 ± 36.3*	100.0 ± 79.8
Iron-deficient	314.3 ± 166.7	217.9 ± 102.8	210.8 ± 126.0
Liver	**ferroportin**	**TfR1**	**hepcidin**
$TNF^{\Delta ARE/+}$			
Iron-adequate	105.9 ± 24.3*	218.3 ± 75.7*+	138.4 ± 79.8*
Iron-deficient	43.8 ± 13.5+	407.7 ± 67.0+	2.3 ± 2.6
Wild-type			
Iron-adequate	100.0 ± 14.0	100.0 ± 22.1*	100.0 ± 35.9*
Iron-deficient	87.6 ± 34.0	815.5 ± 200.1	0.5 ± 0.4
Spleen	**ferroportin**	**TfR1**	**hepcidin** (very low absolute values)
$TNF^{\Delta ARE/+}$			
Iron-adequate	70.1 ± 11.2	68.5 ± 46.6	25.9 ± 16.2*+
Iron-deficient	92.3 ± 20.0	69.1 ± 22.1	92.2 ± 22.4
Wild-type			
Iron-adequate	100.0 ± 47.4	100.0 ± 36.5	100.0 ± 48.0
Iron-deficient	71.1 ± 40.0	87.0 ± 43.8	119.9 ± 112.8

Values are given in percent of those determined in corresponding iron-adequate wild-type-mice.

* Significant difference between corresponding iron-deficient and iron-adequate groups.
+ Significant difference between corresponding wild-type- and $TNF^{\Delta ARE/+}$ groups.

Table 6
Proteins expression in duodenum, spleen, and liver from $TNF^{\Delta ARE/+}$-mice (n=3–5) and wild-type-mice (n=3–5) (M ± SD).

Duodenum	**ferroportin**	**TfR1**	**DMT-1**	
$TNF^{\Delta ARE/+}$				
Iron-adequate	85 ± 30 (n=4)*	90 ± 62 (n=4)	139 ± 17 (n=4)*	
Iron-deficient	550 ± 80 (n=3)	141 ± 30 (n=3)	397 ± 97 (n=3)	
Wild-type				
Iron-adequate	90 ± 180 (n=3)*	100 ± 45 (n=3)	100 ± 34 (n=3)*	
Iron-deficient	1000 ± 450 (n=4)	120 ± 19 (n=4)	396 ± 86 (n=4)	
Liver	**ferroportin**	**TfR1**	**IRP2**	**ferritin**
$TNF^{\Delta ARE/+}$				
Iron-adequate	480 ± 90 (n=3)+	119 ± 7 (n=4)	75 ± 10 (n=4)	95 ± 45 (n=4)*
Iron-deficient	450 ± 100 (n=4)	118 ± 18 (n=4)	115 ± 45 (n=4)+	0 (n=4)
Wild-type				
Iron-adequate	100 ± 190 (n=4)*	100 ± 7 (n=4)*	100 ± 15 (n=4)*	100 ± 35 (n=5)*
Iron-deficient	605 ± 20 (n=3)	130 ± 12 (n=5)	205 ± 30 (n=5)	0 (n=5)
Spleen	**ferroportin**	**TfR1**	**IRP2**	**ferritin**
$TNF^{\Delta ARE/+}$				
Iron-adequate	80 ± 45 (n=3)	230 ± 75 (n=5)+	160 ± 5 (n=5)+	390 ± 420 (n=5)*
Iron-deficient	140 ± 5 (n=3)+	290 ± 70 (n=3)	205 ± 45 (n=3)	0 (n=3)
Wild-type				
Iron-adequate	100 ± 40 (n=4)*	100 ± 70 (n=4)*	100 ± 45 (n=4)	100 ± 160 (n=3)*
Iron-deficient	180 ± 10 (n=4)	365 ± 50 (n=4)	205 ± 80 (n=4)	0 (n=4)

Data represent densitometric evaluation of Western blots, normalized to the values of β-actin, as percent of control.

* Significant difference between corresponding iron-deficient and iron-adequate groups.
+ Significant difference between corresponding wild-type- and $TNF^{\Delta ARE}$-groups.

with one exception, the differences to iron-adequate mice were not significant. Moreover, duodenal TfR1 expression showed no differences between $TNF^{\Delta ARE/+}$ and wild-type-mice. In liver and spleen from iron-deficient wild-type-mice TfR1-expression was significantly higher than in iron-adequacy. In $TNF^{\Delta ARE/+}$ mice these values remained higher than in iron-adequate wild-type controls. Correspondingly, hepatic and splenic ferritin levels were significantly higher in iron-adequate than in iron-deficient mice, where ferritin was virtually not detectable by Western blotting. The content of iron regulatory protein 2 (IRP2) in liver and spleen was increased in iron-deficiency, though significance was reached only in the liver of wild-type animals. Hepatic IRP2 levels tended to be lower in $TNF^{\Delta ARE/+}$ than in wild-type-mice.

Discussion

Duodenal iron transport and expression of iron-related proteins

In iron deficiency, the well-established significant induction in duodenal ^{59}Fe-absorption [20,26,27] correlates with increased expression of ferroportin and DMT-1 [10,28–30]. In iron adequacy, liver-derived circulating hepcidin reduces the number of active ferroportin molecules and diminishes iron-export from duodenal enterocytes (and macrophages) [3,31].

As expected, the increased iron-absorption documented in iron-deficient TNF$^{\Delta ARE/+}$ and wild type mice here (Table 2), was accompanied by increased duodenal DMT-1 and ferroportin protein levels and significantly reduced hepatic hepcidin mRNA-expression (Tables 5 and 6). These molecular responses contribute to the increased lumen-to-body ^{59}Fe-transport in iron-deficiency. Nevertheless, under iron-deficient conditions, we also observed increased duodenal ^{59}Fe-tissue retention (Table 2). At first glance, this may appear paradoxical; however, during steady-state lumen-to-body iron transport, the duodenal ^{59}Fe-content consists of two fractions: the larger part is rapidly transferred to the body [32,33], while a smaller fraction is retained in the duodenal tissue. The transferable ^{59}Fe-fraction is significantly increased in iron-deficiency [34,35], suggesting that iron-deficient duodena increase luminal ^{59}Fe-uptake to a larger extent than basolateral ^{59}Fe-export. Indeed, DMT1 mRNA-level increased 3.9-fold in iron-deficient C57BL6-mice in an earlier trial, as compared to a 2.2-fold increase in ferroportin mRNA [36]. This observation would explain the higher duodenal ^{59}Fe-tissue retention during steady-state iron absorption in iron-deficient mice (Table 2 and [34,35]). Our ferroportin and DMT-1 expression data in wild-type mice show similar increments in iron-deficiency as in Ref. [36]; though duodenal ferroportin increments appeared slightly higher than those of DMT-1 (Table 6).

^{59}Fe-transport across the basolateral membrane (Table 2, left column) depends on the ^{59}Fe-content of the duodenal cell (Table 2, right column) and on the duodenal ferroportin-1 expression level (Table 6). The values suggest that the rate obeys a second-order rate law

$$\text{rate} = k * \text{Fe} * \text{ferroportin},$$

where rate is the lumen-to-body transport rate [pmol/cm/min], Table 2, left column, Fe the iron concentration (retention level [nmol/cm]), Table 2, right column, ferroportin the ferroportin level (dimensionless units), Table 6 (ferroportin in duodenum), k the apparent rate constant [$\text{min}^{-1} * 10^{-3}$].

Such theoretic model calculations lead to apparent rate constants of ~0.08 for iron-adequate wild-type- and TNF$^{\Delta ARE/+}$-mice and of ~0.028 in iron-deficiency (calculation example for wild-type, iron-deficient diet: k=42.8/1.52/1000=0.028 – see Tables 2 and 6). These figures contain a hypothetic component, though, by assuming that the total duodenal ^{59}Fe-content and all ferroportin-1 molecules participate in duodenal iron export. This is not necessarily so. Earlier assessment of the exportable duodenal ^{59}Fe-fraction showed an up to 6-fold increment in iron-deficiency [34]. Whether this is high enough to explain the approx. 10-fold increment in ^{59}Fe-lumen-to-body transport rates (Table 2) may be doubted. Thus, the analysis suggests that additional components may be engaged. Independent from such absolute values for rate constants which contain theoretical assumptions the model demonstrates that an increase in duodenal ^{59}Fe-content can compensate for a reduction in ferroportin-1 activity and *vice versa* regarding the rate of ^{59}Fe lumen-to-body transport.

Surprisingly, inflammation in iron-adequate TNF$^{\Delta ARE/+}$ mice affected duodenal ferroportin expression neither at the mRNA- nor at the protein-level, while DMT-1 protein levels remained unaltered as well (Tables 5 and 6). Hepatic hepcidin-1 mRNA expression slightly increased in TNF$^{\Delta ARE/+}$ mice, though these increments failed to reach significance (Table 5). These findings are in agreement with *in vitro* data showing that TNFα is not a strong, direct hepcidin inducer [37].

Iron-deficient TNF$^{\Delta ARE/+}$ mice showed significantly higher duodenal ^{59}Fe-tissue retention than wild-types (Table 2). These findings suggest a reduced ferroportin-mediated duodenal export of recently absorbed ^{59}Fe in inflammation, in agreement with the apparently lower ferroportin levels (Table 6). Accordingly, duodenal ^{59}Fe-retention in iron-deficiency increased to a comparable extent in TNF$^{\Delta ARE/+}$ mice (4.0-fold) and in wild-types (3.5-fold), while ^{59}Fe-transfer to the body increased less in TNF$^{\Delta ARE/+}$ mice (8-fold) than in wild-type-mice (14-fold) (Table 2). As the increment in duodenal ^{59}Fe-content became significant only in iron-deficient TNF$^{\Delta ARE/+}$ mice, the corresponding increase in DMT-1 seems to contribute to this process as well. The kinetic model calculation provided above is not based on sufficient information to judge on the contribution of DMT-1 mediated ^{59}Fe-influx, ferroportin-mediated outflux capacities, or intracellular iron distribution phenomena to the regulation of duodenal overall ^{59}Fe-transport. However, it indicates that duodenal ^{59}Fe-content in TNF$^{\Delta ARE/+}$-mice may increase in proportion to decreased ferroportin expression to yield the same transport rate in both genotypes (Table 2). This supports the assumption of second order rate kinetics for duodenal ^{59}Fe-export. However, higher ^{59}Fe-retention in villus-tip enterocytes due to a basolateral hepcidin-induced block may increase ^{59}Fe-losses with enterocytes exfoliation [38,39] and reduce ^{59}Fe-absorption in TNF$^{\Delta ARE/+}$ mice in the long run, so that 15 min ^{59}Fe-absorption experiments may not reflect the long-term absorptive situation.

Body iron distribution and expression of related proteins

^{59}Fe-distribution in wild-type-mice (Table 3) did not differ from values determined in C57BL6-mice in earlier experiments [24]. The lower ^{59}Fe-content in ileum, duodenum, and fur after 14 days as compared to 24 h after ^{59}Fe-injection (Table 3) is due to shedding of enterocytes [40] and skin epithelial cells and, thus, to loss of ^{59}Fe-activity. ^{59}Fe-reduction over time in spleen and bone marrow seem to be caused by the shift of recently absorbed ^{59}Fe from interim splenic storage to erythropoiesis and from there to circulating erythrocytes, as shown earlier [24].

Under inflammatory conditions, hepcidin- and cytokine-mediated ferroportin inhibition impairs iron export [3,4]; thus, it was anticipated that the reticuloendothelial system (RES) in inflamed TNF$^{\Delta ARE/+}$ mice would accumulate more iron. However, splenic ^{59}Fe-retention was not increased in TNF$^{\Delta ARE/+}$ mice (Tables 3 and 4), and photometrically determined splenic non-haem iron content was even significantly lower than in wild-type-mice (Table 1). This suggests a significant shift of iron-loaded RES cells from the spleen into the inflamed tissues. Indeed, ^{59}Fe accumulated in the inflamed joints of hemizygous TNF$^{\Delta ARE/+}$ mice within 24 h even after provision for hyperaemia of inflammation. The inflamed joints and ileal tissue maintained a higher ^{59}Fe-content also under steady state conditions 2 weeks after injection (Table 3; [24]), which is supported by the higher endogenous non-haem iron content determined photometrically. Moreover, as TNF$^{\Delta ARE/+}$ mice become anaemic, extramedullary erythropoiesis will be induced in spleen and liver which affects local iron distribution via incorporation of iron into erythroblast. At the same time, erythropoiesis-driven regulators of iron homoeostasis such as GDF-15 may affect the regulation of hepcidin expression and, thus, body iron homoeostasis [41].

Conclusions

$TNF^{\Delta ARE/+}$ mice allow ferrokinetic and biochemical studies regarding the impact of iron-deficiency and inflammation on systemic iron homoeostasis. In both wild type and $TNF^{\Delta ARE/+}$ mice, iron deficiency increases duodenal iron absorption via higher DMT-1 expression. The relatively lower duodenal ferroportin expression found in $TNF^{\Delta ARE/+}$ mice is expected to limit basolateral iron export in the duodenum which can be compensated by increased ^{59}Fe-quantities in duodenal enterocytes, so that ^{59}Fe lumen-to-body transport remains unimpaired [42]. Shedding of enterocytes with a high load of recently absorbed iron may reduce iron absorption in inflammation. Nevertheless, our results suggest that impaired iron absorption does not exclusively account for iron-limited erythropoiesis in iron-deficient $TNF^{\Delta ARE/+}$ mice. The profound leukocyte infiltration (Fig. 1) indicates that at least part of the ^{59}Fe that accumulates in inflamed tissue derives from iron-rich RES cells recruited from the spleen. Our data are consistent with the idea that chronic inflammation modulates systemic iron homoeostasis and erythropoiesis by complex and partially redundant pathways and mechanisms.

Acknowledgement

We thank Prof. George Kollias and the Biomedical Sciences Research Centre "Alexander Fleming" for the permission to work with their $TNF^{\Delta ARE}$-mice. The study was financed and supported by a collaborative grant to KS and KP from the *Bayrische Staatkanzlei* (CI 2.3-020180-4-14-325; Projekt Nr. 09.314) and the Quebec *Ministère de la Recherche, de la Science et de la Technologie* (PSSIRI-011) and the Hildegard-Grunow-Foundation, Munich. The authors thank Tina Hallas for her expert support in animal breeding and in carrying out the experiments on iron kinetics, as well as Bill Andriopoulos and Anja Hausmann for analysis of tissue samples.

Appendix A. Supporting information

Supplementary data associated with this article can be found in the online version at doi:10.1016/j.jtemb.2009.10.002.

References

[1] Weiss G, Goodnough LT. Anemia of chronic disease. N Engl J Med 2005;352:1011–23.
[2] Brissot P, Troadec MB, Loreal O. The clinical relevance of new insights in iron transport and metabolism. Curr Hematol Rep 2004;3:107–15.
[3] Nemeth E, Tuttle MS, Powelson J, Vaughn MB, Donovan A, Ward DM, Ganz T, Kaplan J. Hepcidin regulates cellular iron efflux by binding to ferroportin and inducing its internalization. Science 2004;306:2090–3.
[4] Ludwiczek S, Aigner E, Theurl I, Weiss G. Cytokine mediated regulation of iron transport in human monocytic cells. Blood 2003;101:4148–54.
[5] Weiss G, Bogdan C, Hentze MW. Pathways for the regulation of macrophage iron metabolism by the anti-inflammatory cytokines IL-4 and IL-13. J Immunol 1997;158:420–5.
[6] Pantopoulos K, Weiss G, Hentze MW. Nitric oxide and oxidative stress (H_2O_2) control mammalian iron metabolism by different pathways. Mol Cell Biol 1996;16:3781–8.
[7] Torti FM, Torti SV. Regulation of ferritin genes and protein. Blood 2002;99:3505–16.
[8] Yang F, Liu XB, Quinines M, Melby PC, Ghio A, Haile DJ. Regulation of reticuloendothelial iron transporter MTP1 (Slc11a3) by inflammation. J Biol Chem 2002;277:39786–91.
[9] Theurl I, Theurl M, Seifert M, Mair S, Nairz M, Rumpold H, Zoller H, Bellmann-Weiler R, Niederegger H, Talasz H, Weiss G. Autocrine formation of hepcidin induces iron retention in human monocytes. Blood 2008;111:2392–9.
[10] Pigeon C, Courselaud B, Leroyer P, Turlin B, Brissot P, Loréal O. A new mouse liver-specific gene, encoding a protein homologous to human antimicrobial peptide hepcidin, is overexpressed during iron overload. J Biol Chem 2001;276:7811–9.
[11] Johnson D, Bayele H, Johnston K, Tennant J, Srai SK, Sharp P. Tumour necrosis factor alpha regulates iron transport and transporter expression in human intestinal epithelial cells. FEBS Lett 2004;573:195–201.
[12] Means RT. Recent developments in the anemia of chronic disease. Curr Hematol Rep 2003;2:116–21.
[13] Friedman S, Blumberg RS. Inflammatory bowel disease. In: Kasper DL, Fauci AS, Longo DL, Braunwald E, Hauser SL, Jameson JL, editors. Harrison's Principles of Internal Medicine, 16th ed.. New York: McGraw Hill Medical Publishing Division; 2005. p. 1776–89.
[14] Gasche C, Lomer MC, Cavill I, Weiss G. Iron, anaemia, and inflammatory bowel diseases. Gut 2004;53:1190–7.
[15] Kontoyiannis D, Pasparakis M, Pizarro TT, Cominelli F, Kollias G. Impaired on/off regulation of TNF biosynthesis in mice lacking TNF AU-rich elements: implications for joint and gut-associated immunopathologies. Immunity 1999;10:387–98.
[16] Seril DN, Liao J, Ho KLK, Warsi A, Yang CS, Yang G-Y. Dietary iron supplementation enhances DSS-induced colitis and associated colorectal carcinoma developments in mice. Digest Dis Sci 2002;47:1266–78.
[17] Schümann K, Elsenhans B, Hunder G, Strugala G, Forth W. Increase of the intestinal iron absorption in growing rats and mice after 8 days of iron-deficient feeding. Z Versuchstierkd 1989;32:261–7.
[18] Torrance JD, Bothwell TH. A simple technique for measuring storage iron concentrations in formalinised liver samples. S Afr J Med Sci 1968;33:9–11.
[19] Hermanns W, Liebig K, Schulz LC. Postembedding immunohistochemical demonstration of antigen in experimental polyarthritis using plastic embedded whole joints. Histochemistry 1981;73:439–46.
[20] Bahram S, Gilfillan S, Kühn LC, Moret R, Schulze JB, Lebeau A, Schümann K. Experimental hemochromatosis due to MHC class I HFE deficiency: immune status and iron metabolism. PNAS 1999;96:13312–7.
[21] Ludwiczek S, Theurl I, Bahram S, Schumann K, Weiss G. Regulatory networks for the control of body iron homeostasis and their dysregulation in HFE mediated hemochromatosis. J Cell Physiol 2005;204:489–99.
[22] Chen G, Fillebeen C, Wang J, Pantopoulos K. Overexpression of iron regulatory protein 1 suppresses growth of tumor xenografts. Carcinogenesis 2007;28:785–91.
[23] Fillebeen C, Muckenthaler M, Andriopoulos B, Bisaillon M, Mounir Z, Hentze MW, Koromilas AE, Pantopoulos K. Expression of the subgenomic hepatitis C virus replicon alters iron homeostasis in Huh7 cells. J Hepatol 2007;47:12–22.
[24] Schümann K, Szegner B, Kohler B, Pfaffl M, Ettle T. A method to assess ^{59}Fe in residual tissue blood content in mice and its use to correct ^{59}Fe-distribution kinetics accordingly. Toxicology 2007;241:19–32.
[25] Szegner B, Herbach N, Ettle T, Elsenhans B, Schümann K. Assessing and influencing the fractional contribution of erythrocyte-bound ^{59}Fe to individual ^{59}Fe tissue content in murine ^{59}Fe distribution studies. Toxicology 2007;244:198–208.
[26] Pirzio-Biroli G, Finch CA. Iron absorption. III. The influence of the iron stores on iron absorption in the normal subject. J Lab Clin Med 1960;55:216–20.
[27] Schümann K, Elsenhans B, Ehtechami C, Forth W. Rat intestinal iron transfer capacity and the longitudinal distribution of its adaptation to iron-deficiency. Digestion 1990;46:35–45.
[28] Donovan A, Brownlie A, Zhou Y, Shepard J, Pratt SJ, Maynihan J, Paw BH, Drejer A, Barut B, Zapata A, Law TC, Brugnara C, Lux SE, Pinkus GS, Pinkus JL, Kingsley PD, Palis J, Fleming MD, Andrews NC, Zon LI. Positional cloning of zebrafish ferroportin 1 identifies a conserved vertebrate iron exporter. Nature 2000;403:776–81.
[29] McKie AT, Marciani P, Rolfs A, Brennan K, Wehr K, Barrow D, Miret S, Bomford A, Peters TJ, Farzaneh F, Hediger MA, Hentze MW, Simpson RJ. A novel duodenal iron-regulated transporter IREG1, implicated in the basolateral transfer of iron to the circulation. Mol Cell 2000;5:299–309.
[30] Donovan A, Lima CA, Pinkus GS, Zon LI, Robino S, Andrews NC. The iron exporter ferroportin/Slc 40a1 is essential for iron homeostasis. Cell Metab 2005;1:191–200.
[31] Chaston T, Chung B, Mascarenhas M, Marks J, Patel B, Srai SK, Sharp P. Evidence for differential effects of hepcidin in macrophages and intestinal epithelia cells. Gut 2008;57:374–82.
[32] Wheby MS, Crosby WH. The gastrointestinal tract and iron absorption. Blood 1963;22:416–28.
[33] Wheby MS, Jones LG, Crosby WH. Studies on iron absorption. Intestinal regulatory mechanisms. J Clin Invest 1964;43:1433–42.
[34] Schümann K, Elsenhans B, Forth W. Kinetic analysis of ^{59}Fe-movement across the intestinal wall in duodenal rat segments ex vivo. Am J Physiol 1999;276:G431–0.
[35] Simpson RJ. Dietary iron levels and hypoxia independently affect iron absorption in mice. J Nutr 1996;126:1858–64.
[36] Dupic F, Fruchon S, Bensaid M, Loreal O, Brissot P, Borot N, Roth MP, Coppin H. Duodenal mRNA expression of iron related genes in response to iron loading and iron deficiency in four strains of mice. Gut 2002;51:648–53.
[37] Nemeth E, Valore EV, Territo M, Schiller G, Lichtenstein A, Hepcidin Ganz T. a putative mediator of anaemia of inflammation, is a type II acute-phase protein. Blood 2003;101:2461–3.
[38] Hunt JR, Roughead ZK. Nonheme-iron absorption, fecal ferritin excretion, and blood indexes of iron status in women consuming controlled lactovegetarian dieta for 8 wk. Am J Clin Nutr 2000;69:944–52.

[39] Sharp P, Srai SK. Molecular mechanisms involved in intestinal iron absorption. World J Gastroenterol 2007;13:4716–24.
[40] Schümann K, Moret R, Künzle H, Kühn LC. Iron regulatory protein as an endogenous sensor of iron in rat intestinal mucosa. Possible implications for the regulation of iron absorption. Eur J Biochem 1999;260: 362–72.
[41] Tanno T, Bhanu NV, Oneal PA, Goh SH, Staker P, Lee YT, Moroney JW, Reed CH, Luban NL, Wang RH, Eling TE, Childs R, Ganz T, Leitman SF, Fucharoen S, Miller JL. High levels of GDF15 in thalassemia suppress expression of the iron regulatory protein hepcidin. Nat Med 2007;13:1096–101.
[42] Hentze MW, Muckenthaler MU, Andrews NC. Balancing acts: molecular control of mammalian iron metabolism. Cell 2004;117:285–97.